

# Influence of pH and Surface Chemistry on Poly(L-lysine) Adsorption onto Solid Supports Investigated by Quartz Crystal Microbalance with Dissipation Monitoring

Jae-Hyeok Choi,<sup>†,‡</sup> Seong-Oh Kim,<sup>†,‡</sup> Eric Linardy,<sup>†,‡</sup> Erik C. Dreaden,<sup>§</sup> Vladimir P. Zhdanov,<sup>†,‡,⊥</sup> Paula T. Hammond,<sup>§</sup> and Nam-Joon Cho<sup>\*,†,‡,||</sup>

<sup>†</sup>School of Materials Science and Engineering, Nanyang Technological University, 50 Nanyang Avenue, 639798 Singapore

<sup>‡</sup>Centre for Biomimetic Sensor Science, Nanyang Technological University, 50 Nanyang Drive, 637553 Singapore

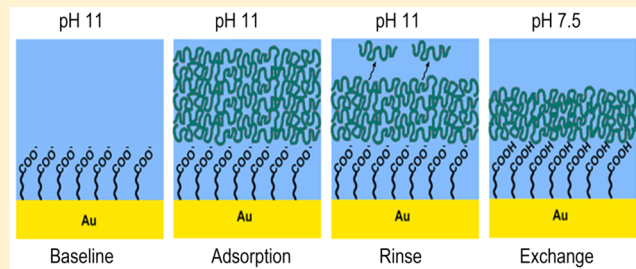
<sup>§</sup>Koch Institute for Integrative Cancer Research, Department of Chemical Engineering, Institute for Soldier Nanotechnologies, Massachusetts Institute of Technology, 500 Main Street, Cambridge, Massachusetts 02139, United States

<sup>||</sup>School of Chemical and Biomedical Engineering, Nanyang Technological University, 62 Nanyang Drive, 637459 Singapore

<sup>⊥</sup>Boreskov Institute of Catalysis, Russian Academy of Sciences, Novosibirsk 630090, Russia

## Supporting Information

**ABSTRACT:** Poly(L-lysine) (PLL) adsorption onto various materials has been widely applied as a surface modification strategy and layer-by-layer fabrication method. Considering the role of electrostatic charges, a detailed understanding of the influence of solution pH on PLL adsorption process is important for optimization of PLL coating protocols. Herein, PLL adsorption onto different polar and hydrophilic substrates—silica, an amine-terminated self-assembled monolayer (SAM) on gold, and a carboxyl-terminated SAM on gold—across a range of pH conditions was investigated using the quartz crystal microbalance with dissipation. The adsorption kinetics consisted of an initial rapid phase, followed by a second phase where adsorption rate gradually decelerated. These features were interpreted by applying a mean-field kinetic model implying diffusion-limited adsorption in the first phase and reconfiguration of adsorbed PLL molecules in the second phase. The adsorption kinetics and uptake were found to be sensitive to the pH condition, surface chemistry, and flow rate. The strongest PLL adsorption occurred at pH 11 on all three surfaces while weak PLL adsorption generally occurred under acidic conditions. The surface morphology and roughness of adsorbed PLL layers were investigated using atomic force microscopy, and strong PLL adsorption is found to produce a uniform and smooth adlayer while weak adsorption formed a nonuniform and rough adlayer.



## INTRODUCTION

Absorption of polypeptides onto solid supports plays an important role in engineering biomaterial interfaces. One representative example is poly(L-lysine) (PLL), which is a polymer composed of lysine amino acids. Owing to its attractive properties, including hydrophilicity, excellent biocompatibility, and biodegradability, PLL has been widely utilized for biomaterial applications<sup>1,2</sup> such as surface coatings,<sup>3–9</sup> drug,<sup>10–12</sup> gene,<sup>13,14</sup> and protein<sup>15</sup> delivery platforms and hydrogel scaffolds.<sup>16</sup> In particular, PLL-coated materials support adhesion of cells,<sup>3</sup> nucleic acids,<sup>7</sup> peptides,<sup>6,8</sup> and enzymes.<sup>7,9</sup> PLL has also been utilized as a component in layer-by-layer multilayer assemblies,<sup>17–19</sup> and can improve attachment of less adhesive polymers (e.g., poly(ethylene glycol)<sup>8,20,21</sup>) through grafting. Indeed, PLL is known to spontaneously adsorb onto various types of materials, including glass,<sup>3,22</sup> metals,<sup>4,8</sup> polymers,<sup>6,21</sup> and metallic oxides.<sup>5,23–27</sup>

Mechanistically, adsorption of PLL is similar to that of other polyelectrolytes.<sup>20,28,29</sup> In analogy with proteins,<sup>30–34</sup> it occurs

via two main steps: (i) diffusion of polyelectrolyte from the bulk solution and attachment of polyelectrolyte to the surface and (ii) rearrangement of polyelectrolytes in the adlayer.<sup>29,35–38</sup> The latter step may involve intramolecular charge and hydrogen bond redistribution and molecular aggregation as articulated in recent studies.<sup>29,35–38</sup> According to the literature, there is a general view that these steps are mainly governed by the electrostatic interaction between the polyelectrolyte and the substrate and the electrostatic repulsion between the polyelectrolyte chains.<sup>18,20,26,27</sup> As a result, the adsorption rate and total uptake depend on the charges of the functional groups on both PLL and the substrate, and accordingly, the whole process is sensitive to changes in pH, temperature, and ionic strength of the solution.<sup>20,26,27</sup> In particular, previous studies<sup>26,27</sup> have demonstrated that from pH 4 to 12 PLL

Received: February 15, 2015

Revised: June 10, 2015

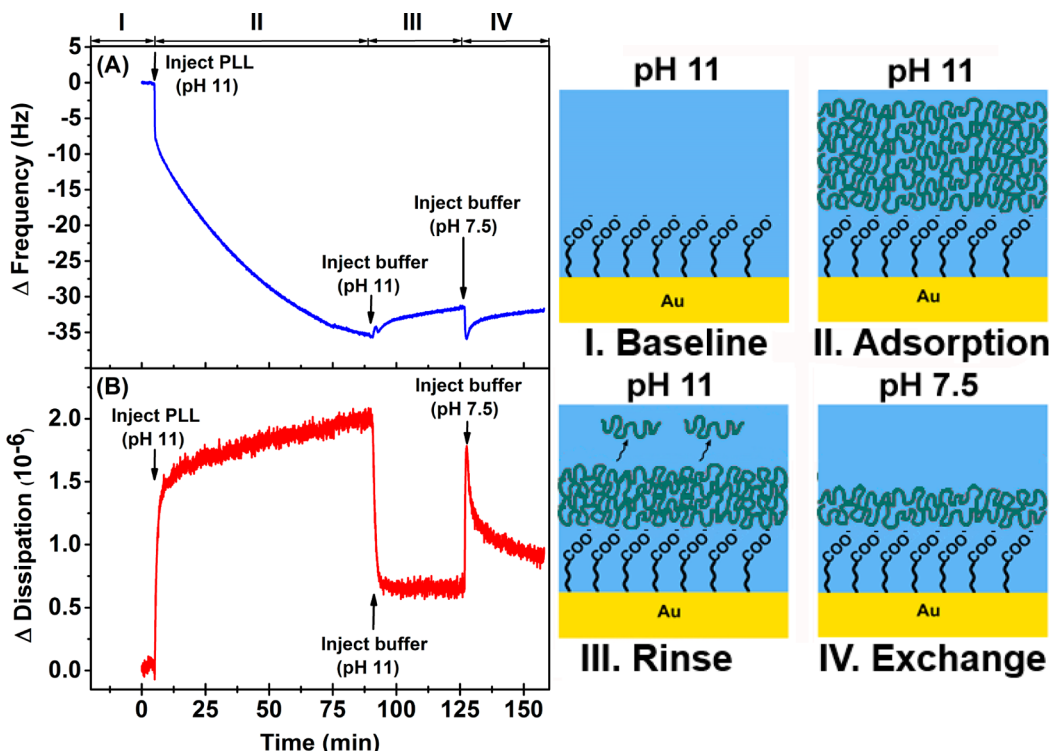


**Figure 1.** Representative kinetics of poly(*L*-lysine) (PLL) self-assembly on carboxyl-functionalized gold surface. The QCM-D measurement technique was utilized to monitor the (A) frequency and (B) dissipation response kinetics for PLL self-assembly on the surface as a function of time. After initial stabilization and measurement of baseline in Tris buffer solution at pH 11 (I, Baseline), PLL solution was injected at pH 11 at  $t = 5$  min for about 70 min (II, Adsorption). The surface of the substrate was then left to incubate for about 10 min, followed by rinsing with Tris buffer solution at equivalent pH (pH 11) at  $t = 90$  min for 35 min (III, Rinse). Lastly, solution exchange to Tris buffer solution at near-physiological pH (pH 7.5) at  $t = 125$  min until the end of assembly process (IV, Exchange). Corresponding schematics illustrate the process of assembly of PLL on carboxyl-functionalized gold surface.

uptake on silica generally increases with the solution pH, which is consistent with an electrostatic mechanism. In this context, one may notice that silica has a low isoelectric point (IEP) of approximately 4,<sup>39</sup> while the  $pK_a$  of PLL has been reported to range from 9 to 11.<sup>4,20,27,40,41</sup> Hence, PLL is cationic at acidic and neutral pH,<sup>27</sup> and accordingly, an electrostatic attraction between PLL and the surface is present under physiological conditions. On the other hand, the  $pK_a$  of other surfaces functionalized with carboxyl- and amine-functionalized self-assembled monolayer (SAM) are about 6 and 7.5, respectively.<sup>42–45</sup> At the same time, solution pH is also known<sup>46–48</sup> to influence the conformation of PLL molecules, although a relationship between the conformational state of PLL in solution and its adsorption properties has not been established.

At the molecular level, the conformational state of PLL is determined by hydrogen bonds and the degree of electrostatic repulsion between its side chains.<sup>4,20,22,40,41</sup> For example, under acidic conditions, PLL chains in aqueous solution adopt a random coil conformation due to strong electrostatic repulsion between the protonated chains. With a gradual increase in pH, the conformation gradually transforms into  $\alpha$ -helical domains, in response to the reduction in electrostatic repulsion as the side chains become increasingly deprotonated. After adsorption<sup>4,26,41</sup> or incorporation into polyelectrolyte multilayers,<sup>40</sup> the PLL secondary structure may further change due to PLL–surface or PLL–polyanion interactions. With changes in the conformational state, the corresponding macroscopic properties of PLL such as wettability,<sup>49</sup> degree of swelling,<sup>26</sup> and refractive index<sup>41</sup> may also change and be utilized in the fabrication of

stimuli-responsive materials for various applications.<sup>4,49,50</sup> Taken together, these points emphasize the need to expand our understanding of the process of PLL adsorption on a wide range of substrates, thereby clarifying molecular-level details and translating this knowledge into improved surface modification strategies.

The objective of the present work is to investigate PLL adsorption onto different substrates including silica, an amine-terminated SAM on gold, and a carboxyl-terminated SAM on gold across a wide range of pH conditions from 2 to 12. The deposition of PLL on the substrates was studied using a three-step protocol: (i) adsorption of polyelectrolyte at a specific pH, (ii) buffer rinsing at similar pH, and then (iii) solution exchange to near-neutral aqueous buffer conditions. The assembly process was monitored using quartz crystal microbalance with dissipation (QCM-D) technique in order to investigate adsorption kinetics and PLL uptake. A phenomenological model was employed to describe the kinetics of the experimentally observed adsorption and buffer rinsing phases. In addition, the surface morphology of the PLL adlayers was investigated using atomic force microscopy (AFM).

## MATERIALS AND METHODS

**Polyelectrolyte and Buffer Solutions.** Tris buffer solutions (10 mM Tris, 150 mM NaCl) were prepared by dissolving Tris (6947, Ultra Pure grade, 99% purity, Amresco) and sodium chloride (S7653 BioXtra, 99.5% purity, Sigma-Aldrich) in Milli-Q water. The pH of the buffer solution was adjusted to various pH between 2 and 12 via titration with 1 M

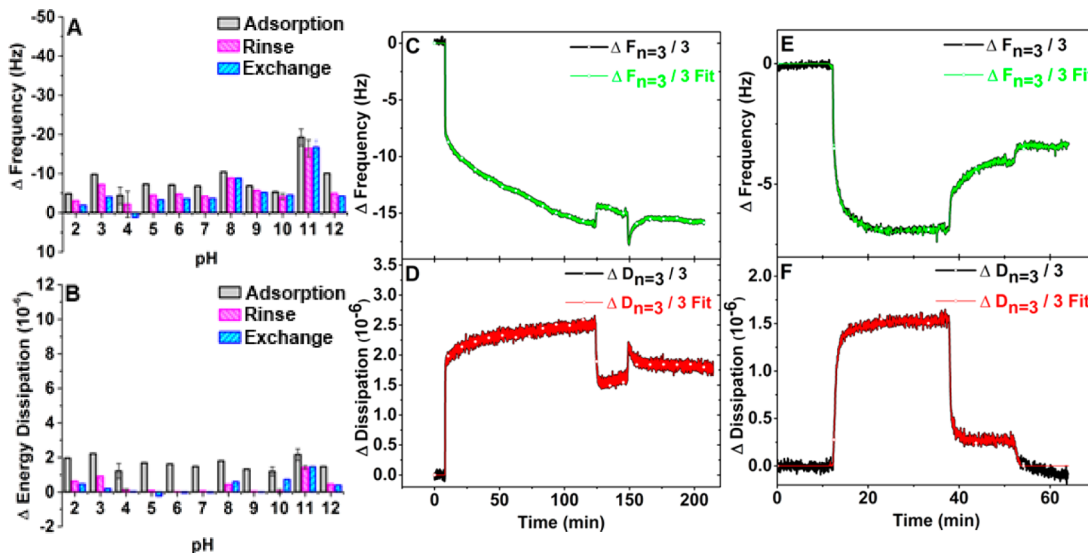


**Figure 2.** Influence of pH on PLL adsorption kinetics on silica. Summary of QCM-D (A) frequency and (B) energy dissipation shifts corresponding to each protocol step (adsorption, rinse, exchange) are presented across the range of tested pH conditions. Representative kinetics for a strong adsorption case (pH 11) are exhibited in panels C and D. Similar data are also shown for a weak adsorption (pH 5) in panels E and F.

hydrochloric acid (HCl) or 1 M sodium hydroxide (NaOH). The pH of the buffer solution was checked before experiment. PLL solutions at different pH between 2 and 12 were prepared at high concentration (77 mg/mL) by dissolution of PLL (P-6516, Sigma-Aldrich, 4–15 kDa, with monomer size of ~146 Da) in Tris buffer at specific pH followed by vortexing for 30 min. The concentrated PLL solutions were diluted to 2 mg/mL with Tris buffer at the same pH immediately prior to use.

**Quartz Crystal Microbalance with Dissipation (QCM-D) Monitoring.** The adsorption of PLL was monitored using QCM-D (Q-Sense E4, Biolin Scientific, Göthenburg, Sweden) and recorded at several different overtones ( $n = 3, 5, 7, 9, 11$ ). Gold (QSX301) and silica (QSX303) coated QCM-D substrates were used (Biolin Scientific). Both substrates were exposed to oxygen plasma (Harrick Plasma, Ithaca, NY) for 1 min. Gold substrates were then functionalized with either 11-mercaptopundecanoic acid (MUA) (450561, 95% purity, Sigma-Aldrich) or 11-amino-1-undecanethiol hydrochloride (AUT) (674397, 99% purity, Sigma-Aldrich). MUA and AUT were dissolved in absolute ethanol (100983, Merck Millipore). Previously cleaned gold substrates were incubated in 1 mM of MUA and AUT ethanolic solutions overnight at 4 °C and then removed and rinsed with 70% ethanol, Milli-Q water, and 70% ethanol, in that order. The functionalized gold substrates were then dried with nitrogen gas. QCM-D experimental results were analyzed using the Sauerbrey<sup>18</sup> and Voigt-based viscoelastic models.<sup>51</sup> The Sauerbrey model was employed to determine the surface concentration ( $\Delta m$ ) of the adsorbed PLL on the surface for the kinetic model fitting, according to the equation

$$\Delta m = -C \frac{\Delta f_n}{n}$$

where  $\Delta f_n$  is the shifts in frequency,  $n$  is the overtone number, and  $C$  is the mass sensitivity constant where  $C \approx 17.7 \text{ ng cm}^{-2} \text{ Hz}^{-1}$  with fundamental frequency of about 5 MHz in air. The Voigt-based viscoelastic model analysis was performed in order to determine the Voigt thickness of the adsorbed PLL film using the QTools software (Biolin Scientific) with fixed

parameters for PLL film density at 1000 kg/m<sup>3</sup> and the density and viscosity of bulk solution at 1000 kg/m<sup>3</sup> and 0.001 Pa/s, respectively.<sup>18</sup>

**Atomic Force Microscopy (AFM).** An atomic force microscope (NX-Bio, Park Systems, South Korea), combined with an optical microscope (Eclipse Ti, Nikon, Japan), was used for contact mode AFM imaging on PLL adlayers formed on QCM-D substrates in buffer environment. A fresh silicon nitride, ultrasharp, AFM tip (0.1 N/m, BioLever mini BL-AC40TS-C2, Olympus) was employed. The AFM and sample were contained in an acoustic enclosure with a temperature controller (Park Systems) set at a constant temperature of 25 °C.

## RESULTS

**QCM-D Characterization of PLL Adlayers on Substrates.** PLL assembly on three substrates with different ionizable functional groups at different pH (from 2 to 12) was monitored with QCM-D. The PLL assembly was performed with the protocol depicted in Figure 1. At the start of the process, a measurement baseline was established in Tris buffer solution at a specific pH (region I). Subsequently, PLL solution at equivalent pH was injected, starting at  $t \approx 5$  min (region II). After 70 min, injection was stopped, and the substrate was left to incubate for about 15 min. Subsequently, buffer rinsing was performed at  $t \approx 90$  min (region III) using the Tris buffer at equivalent pH to remove excess weakly bound PLL molecules from the substrate. The solution exchange to Tris buffer solution at pH 7.5 was then performed at  $t \approx 125$  min, in order to assess the properties of the adsorbed layer in response to near-physiological pH conditions (region IV).

The QCM-D shifts in frequency ( $\Delta f$ ) and energy dissipation ( $\Delta D$ ), which correspond to the mass and viscoelastic properties of the adsorbed PLL layer, respectively, were recorded as a function of time. The final  $\Delta f$  and  $\Delta D$  shifts at the end of each assembly step (i.e., adsorption, buffer rinsing and solution exchange) varied according to the pH of the PLL solution and the surface chemistry of each type of substrate. In the following section, we summarize these shifts and examine two cases for

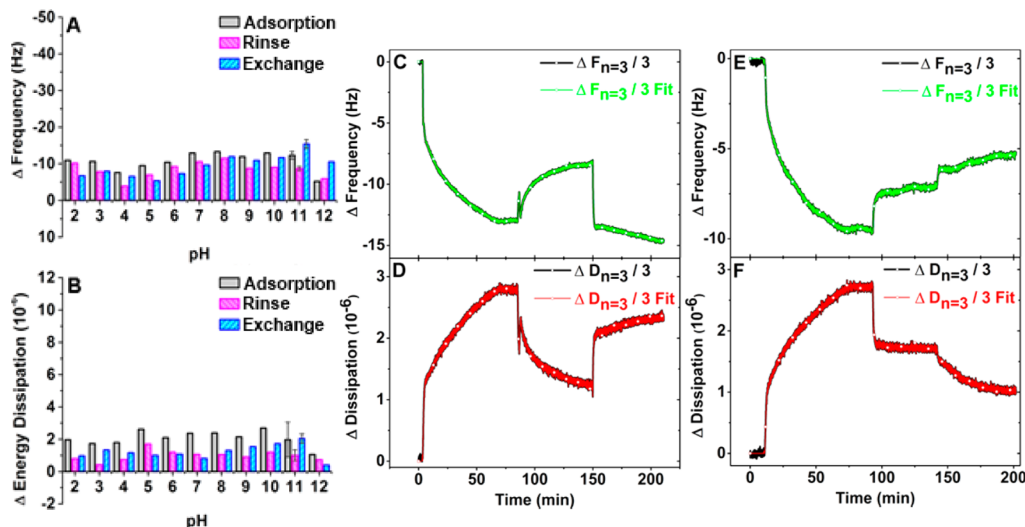


**Figure 3.** Influence of pH on PLL adsorption kinetics on amine-functionalized gold. Summary of QCM-D (A) frequency and (B) energy dissipation shifts corresponding to each protocol step (adsorption, rinse, exchange) are presented across the range of tested pH conditions. Representative kinetics for a strong adsorption case (pH 11) are exhibited in panels C and D. Similar data are also shown for a weak adsorption (pH 5) in panels E and F.

each substrate, representative of pH conditions yielding strong and weak adsorption of PLL molecules.

**Silica.** Figure 2A,B summarizes the resulting  $\Delta f$  and  $\Delta D$  in response to PLL adsorption on silica. The obtained  $\Delta f$  shifts were between  $-4$  and  $-10$  Hz under all pH conditions, except at pH 11 where the  $\Delta f$  shift was appreciably larger and reached  $-19$  Hz. The corresponding  $\Delta D$  shifts were always below  $2.2 \times 10^{-6}$ , indicating that the PLL adsorbate had relatively low viscoelastic character. In general, the rinsing step led to a minimal increase in  $\Delta f$  shift but significant decrease in  $\Delta D$  shift. The exchange of rinsing solution from acidic to near-physiological pH led to significant increase in  $\Delta f$  shifts and decrease in  $\Delta D$  shifts while for solution exchange from basic pH produced sudden decrease in  $\Delta f$  shift and increase in  $\Delta D$  shifts, followed by slow recovery of the signals (Figure 2C–F). In order to scrutinize in more depth the PLL adsorption kinetics recorded at different pH conditions, we selected those representatives of strong (pH 11) and weak adsorption (pH 5). Adsorption at pH 11 occurred in a rapid, nearly linear initial phase for about 8.6 min, resulting in  $\Delta f$  and  $\Delta D$  shifts of  $-8$  Hz and  $1.8 \times 10^{-6}$ , respectively, followed by a more gradual phase, leading to the final  $\Delta f$  and  $\Delta D$  shifts of  $-19.3$  Hz and  $2.2 \times 10^{-6}$ , respectively (Figure 2C,D). Rinsing at pH 11 resulted in the increase of  $\Delta f$  shift to  $-16.5$  Hz and decrease of  $\Delta D$  shift to  $1.4 \times 10^{-6}$ . Voigt-based viscoelastic modeling was performed for the QCM-D adsorption results in order to determine the effective Voigt thickness ( $t_{\text{Voight}}$ ) of the PLL adlayers (see Figures S1–S4 for detailed information). For this particular case (pH 11), the effective  $t_{\text{Voight}}$  decreased from 3.2 to 2.7 nm upon rinsing. PLL adsorption at pH 5 (Figure 2E,F) followed a similar two-phase scenario with initial rapid adsorption for about 12.5 min, resulting in  $\Delta f$  and  $\Delta D$  shifts of  $-3.5$  Hz and  $0.4 \times 10^{-6}$ , respectively, followed by a gradual phase leading to final  $\Delta f$  and  $\Delta D$  shifts of  $-7.3$  Hz and  $1.7 \times 10^{-6}$ , respectively.

Rinsing step led to significant changes in  $\Delta f$  and  $\Delta D$  shifts of  $-4.5$  Hz and  $0.08 \times 10^{-6}$ , respectively. Accordingly,  $t_{\text{Voight}}$  decreased from 2.3 to 0.8 nm, indicating desorption leaving behind a thin and rigid PLL adlayer. The solution exchange step led to a final  $\Delta f$  shift to  $-3.3$  Hz, a negligible  $\Delta D$  shift, and

a  $t_{\text{Voight}}$  value of 0.6 nm. In summary, the  $\Delta f$  response indicates that PLL adsorption on silica occurred largely independent of solution pH, and rinsing led to desorption of weakly adsorbed PLL from the surface. At the end of assembly process, a thin and rigid PLL adlayer was formed on the surface under most pH conditions, with exceptionally thick layer at pH 11.

**Amine-Functionalized Gold.** In general, PLL adsorption onto amine-functionalized gold (Figure 3A,B) led to more uniform and higher magnitude  $\Delta f$  and  $\Delta D$  shifts across the pH range, with the final  $\Delta f$  shifts ranging from  $-10$  to  $-13$  Hz and  $\Delta D$  shifts ranging from  $1.7 \times 10^{-6}$  to  $2.7 \times 10^{-6}$ . Buffer rinsing step at equivalent pH led to an increase in  $\Delta f$  shifts for most pH conditions, except at pH 12, and a decrease in  $\Delta D$  shifts for all pH conditions. Solution exchange to near-neutral aqueous buffer solution from basic condition resulted in sudden and significant decrease in  $\Delta f$  shift and increase in  $\Delta D$  shift (Figure 3C,D) with the exception of the decrease in  $\Delta D$  shift at pH 12. In contrast to the PLL layer response to solution exchange from basic condition on the other two substrates, there is no additional slow increase in  $\Delta f$  shift after the sudden decrease in  $\Delta f$  shifts. Solution exchange from acidic condition (Figure 3E,F) resulted in gradual increase in  $\Delta f$  shift and decrease in  $\Delta D$  shift which correspond to the behavior of PLL layer on the other two substrates. At pH 11, rapid adsorption occurred at about 4.3 min, resulting in  $\Delta f$  and  $\Delta D$  shifts of  $-5.1$  Hz and  $0.85 \times 10^{-6}$ , respectively, followed by a more gradual phase with final  $\Delta f$  and  $\Delta D$  shifts of  $-12.3$  Hz and  $1.97 \times 10^{-6}$ , respectively (Figure 3C,D). Buffer rinsing at pH 11 led to a significant increase in  $\Delta f$  shift to  $-8.7$  Hz and decrease in  $\Delta D$  shift to  $1 \times 10^{-6}$ , respectively, while  $t_{\text{Voight}}$  decreased from 4 to 3.1 nm. Interestingly, in contrast to the silica case, solution exchange in this case induced a decrease in  $\Delta f$  shift to  $-15.4$  Hz and an increase in  $\Delta D$  shift to  $2.05 \times 10^{-6}$ , resulting in the increase in the effective adlayer thickness to 4 nm. At pH 5, the initial rapid linear phase lasted for about 13 min, resulting in  $\Delta f$  and  $\Delta D$  shifts to  $-3.2$  Hz and  $0.98 \times 10^{-6}$ , respectively, followed by a gradual change in  $\Delta f$  shift to  $-9.5$  Hz and  $\Delta D$  shift to  $2.6 \times 10^{-6}$  (Figure 3E,F). Buffer rinsing at pH 5 led to an increase in  $\Delta f$  shift to  $-7$  Hz, a decrease in  $\Delta D$  shift to  $1.7 \times 10^{-6}$ ,

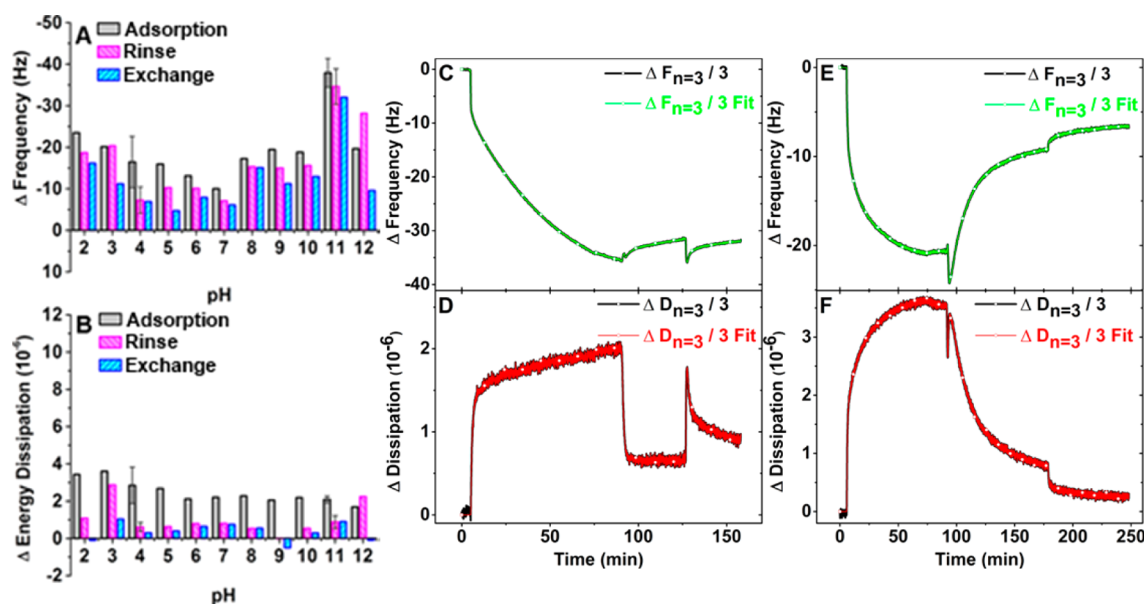


**Figure 4.** Influence of pH on PLL adsorption kinetics on carboxyl-functionalized gold. Summary of QCM-D (A) frequency and (B) energy dissipation shifts corresponding to each protocol step (adsorption, rinse, exchange) are presented across the range of tested pH conditions. Representative kinetics for a strong adsorption case (pH 11) are exhibited in panels C and D. Similar data are also shown for a weak adsorption (pH 4) in panels E and F.

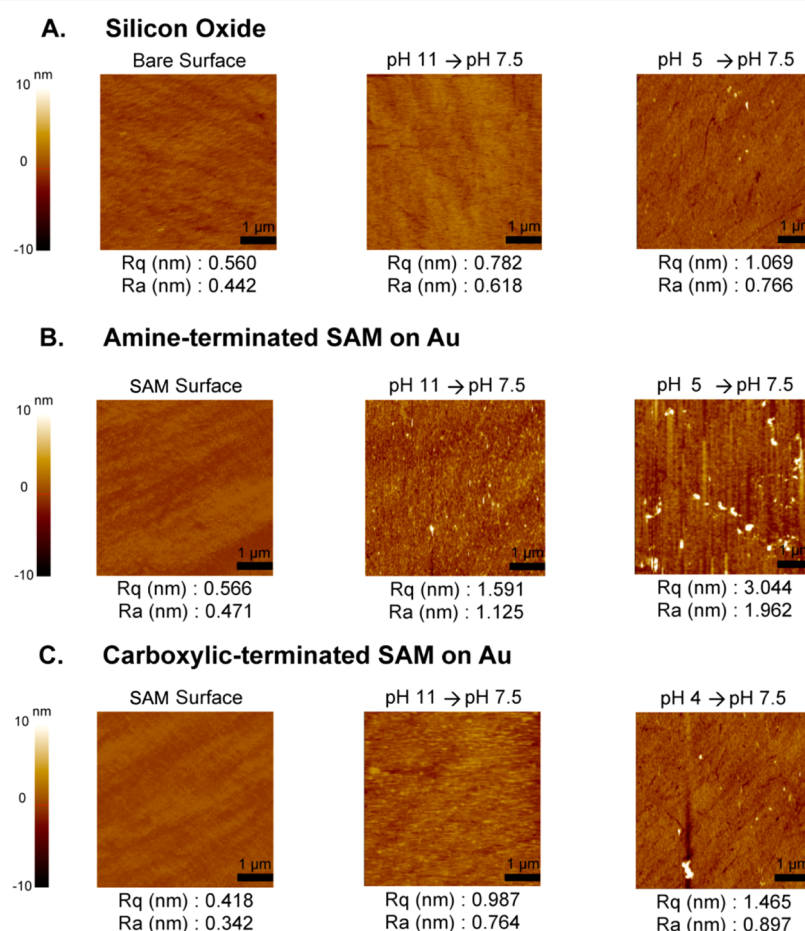


**Figure 5.** AFM images of the bare silica, SAM-functionalized gold, and PLL layers assembled on (a) silicon oxide, (b) amine-functionalized gold, and (c) carboxylic-functionalized gold. For each substrate type, the AFM image of the bare or SAM-functionalized substrate surface (left panel) shows low surface roughness which increased after the complete assembly of the PLL layer at two different adsorption pH conditions, representing the case of strong adsorption (middle panel) and weak adsorption (right panel), respectively. All AFM images are presented within the frame of  $5 \times 5 \mu\text{m}^2$ . The scale bars indicate 1  $\mu\text{m}$ . The height of the white dots exceeds 10 nm.

$10^{-6}$ , and reduction in  $t_{\text{Voight}}$  from 3.5 to 2.2 nm. Solution exchange to pH 7.5 buffer resulted in a further increase in  $\Delta f$  shift to  $-5.3$  Hz and corresponding reduction in  $t_{\text{Voight}}$  to 1.4 nm. In addition, the solution exchange reduced the  $\Delta D$  shift of the PLL adlayer to approximately  $\sim 1 \times 10^{-6}$ .

**Carboxyl-Functionalized Gold.** The  $\Delta f$  shift at the end of adsorption phase increased gradually from  $-24$  to  $-10$  Hz as pH increased from 2 to 7 while  $\Delta D$  shift initially increased from  $3.5 \times 10^{-6}$  to  $3.6 \times 10^{-6}$  from pH 2 to 3 and then gradually decreased to  $2.1 \times 10^{-6}$  at pH 7 (Figure 4A,B). From pH 8 to 12, the  $\Delta f$  shift remained approximately uniform ranging from  $-18$  to  $-20$  Hz with a notable exception at pH 11 where the  $\Delta f$  shift reached the lowest value of  $-37.9$  Hz. On the other hand, the  $\Delta D$  shift remained approximately constant at about  $2 \times 10^{-6}$ . Buffer rinsing generally resulted in increase in  $\Delta f$  shift and decrease in  $\Delta D$  shift. An exception was observed at pH 12 where  $\Delta f$  shift decreased while  $\Delta D$  shift increased upon buffer rinsing. Solution exchange to pH 7.5 on carboxyl-functionalized surface (Figure 4C–F) generally led to  $\Delta f$  and  $\Delta D$  shifts similar to that observed on silica (Figure 2). The representative cases for strong and weak PLL adsorption were selected at pH 11 and 4, respectively. At pH 11, the conventional two-phase kinetics were observed (Figure 4C,D) with a fast nearly linear initial phase for 5.6 min, leading to  $\Delta f$  and  $\Delta D$  shifts to  $-7.8$  Hz and  $0.73 \times 10^{-6}$ , respectively, followed by a more gradual phase with final  $\Delta f$  shift to  $-37.9$  Hz and  $\Delta D$  shift to  $2.1 \times 10^{-6}$ . The  $t_{\text{Voight}}$  of the PLL adlayer at pH 11 on carboxyl-functionalized gold was the highest observed in this study at 10.4 nm. Buffer rinsing at pH 11 led to slight increase in  $\Delta f$  shift to  $-34.6$  Hz and decrease in  $t_{\text{Voight}}$  to 9.2 nm while the  $\Delta D$  shift decreased significantly to about  $0.6 \times 10^{-6}$ . Solution exchange to pH 7.5 buffer from pH 11 resulted in sudden decrease in  $\Delta f$  shift and increase in  $\Delta D$  shift followed by slow recovery of the signal. The initial rapid adsorption phase at pH 4 lasted for about 7 min, leading to  $\Delta f$  and  $\Delta D$  shifts of  $-8.6$  Hz and  $1.7 \times 10^{-6}$ , respectively, followed by gradual phase resulting in final  $\Delta f$  shift to  $-16.5$  Hz and  $\Delta D$  shift to  $2.85 \times 10^{-6}$  (Figure 4E,F). Buffer rinsing resulted in increase  $\Delta f$  shift to  $-7.3$  Hz and  $\Delta D$  shift decreased to  $0.61 \times 10^{-6}$ , and the  $t_{\text{Voight}}$  decreased from 5.7 to 1.9 nm. Solution exchange to pH 7.5 buffer resulted in final  $\Delta f$  and  $\Delta D$  shifts of  $-6.9$  Hz and  $0.3 \times 10^{-6}$ . At the end of the assembly, PLL adlayer with  $t_{\text{Voight}}$  of 1.23 nm remained on the surface.

**Surface Morphology of Bare Silica, SAM-Functionalized, and PLL-Coated Substrates.** Bare silica exhibited uniform surface (Figure 5A, left panel) with relatively low root-mean-square surface roughness ( $R_q$ ) of 0.560 nm and arithmetic roughness ( $R_a$ ) of 0.442 nm. The roughness increased considerably after the assembly of a PLL adlayer at both pH 11 and 5. The surface roughness of the PLL layer adsorbed at pH 5 ( $R_q = 1.069$  nm,  $R_a = 0.766$  nm), representing the weak adsorption case, was higher compared to that at pH 11 ( $R_q = 0.782$  nm,  $R_a = 0.618$  nm), where strong adsorption had occurred. A uniform PLL adlayer covered the surface after assembly at pH 11, consistent with the lower value of surface roughness (Figure 5A, middle panel). In contrast, the PLL adsorption at pH 5 produced a relatively inhomogeneous surface, with several small white spots, presumably depicting PLL self-aggregates with thickness exceeding 10 nm (Figure 5A, right panel). Nevertheless, the surface topography of the PLL adlayer assembled at both pH 11 and 5 on silica in our study was significantly more homogeneous compared to that of the

PLL adlayer assembled on a similar surface at pH 7.3 and similar ionic strength reported in another study.<sup>18</sup>

Similar to silica, the AFM image of amine-functionalized gold substrate depicts a uniform surface (Figure 5B, left panel) with low surface roughness ( $R_q = 0.566$  nm,  $R_a = 0.471$  nm). The roughness increased significantly after the complete assembly of PLL adlayer at pH 11 and pH 5. The PLL adlayer adsorbed at pH 11 on amine-functionalized gold had a more inhomogeneous surface (Figure 5B, middle panel) and higher surface roughness ( $R_q = 1.591$  nm,  $R_a = 1.125$  nm), even in comparison with the adlayers formed at weak adsorption condition at the other substrates. Furthermore, the PLL adlayer formed at pH 5 had much more inhomogeneous surface (Figure 5B, right panel) with higher density of PLL self-aggregates and much higher roughness ( $R_q = 3.044$  nm,  $R_a = 1.962$  nm) compared with the other substrates. These results indicate that the amine-functionalized surface was not suitable for the assembly of uniform PLL adlayers. The AFM images and surface roughness of PLL adlayer on carboxylic-functionalized gold resembled the other two substrates. Carboxylic-functionalized gold exhibited smooth and uniform surface (Figure 5C, left panel) with lower surface roughness ( $R_q = 0.418$  nm,  $R_a = 0.342$  nm), which increased after adsorption of PLL adlayer at both pH 11 and pH 4. At pH 11, the PLL-coated substrate showed uniform surface (Figure 5C, middle panel) with increased surface roughness ( $R_q = 0.987$  nm,  $R_a = 0.764$  nm) compared with the SAM-functionalized substrate, but lower roughness compared with the PLL adlayer adsorbed at pH 4 ( $R_q = 1.465$  nm,  $R_a = 0.897$  nm) with inhomogeneous surface covered with PLL aggregates (Figure 5C, right panel). In summary, the QCM-D and AFM experiments indicate that particularly high PLL uptake was consistently observed at pH 11, rendering the formation of a generally complete, homogeneous, and relatively smoother adlayer in contrast to adsorption under unfavorable acidic conditions. As the three substrates have different electrical charge properties, high adsorption in this case may be triggered by additional factors, e.g., PLL conformation, driving PLL adsorption onto the surface.

**Kinetic Model.** In order to scrutinize phenomenologically the scenario outlined above, we describe the evolution of the PLL surface concentration,  $C$ , as a function of time by using the following conventional mean-field equation:

$$\frac{dC}{dt} = k_a(C)(1 - C/C_{\max})c - k_d(C)C \quad (1)$$

where  $c$  is the PLL bulk concentration, and  $(1 - C/C_{\max})$  is the factor taking saturation into account ( $C_{\max}$  is the surface concentration corresponding to full saturation). This model was recently used to interpret the kinetics of adsorption of hyaluronic acid on various solid supports.<sup>52</sup> As discussed there, its novelty compared to the conventional models is in specification of the adsorption and desorption rate constants,  $k_a(C)$  and  $k_d(C)$ , which are considered to depend on  $C$  due to PLL reconfiguration and lateral PLL–PLL interaction as

$$k_a(C) = \begin{cases} k_a^o & \text{for } C < C_* \\ k_a^o \exp[-A(C - C_*)^m] & \text{for } C > C_* \end{cases} \quad (2)$$

$$k_d(C) = \begin{cases} k_d^o & \text{for } C < C_* \\ k_d^o \exp[B(C - C_*)^n] & \text{for } C > C_* \end{cases} \quad (3)$$

where  $k_a^o$  and  $k_d^o$  are the constants corresponding to the first adsorption phase,  $C_*$  is the concentration corresponding to the

beginning of the second adsorption phase, and  $n$ ,  $m$ ,  $A$ , and  $B$  are exponents and positive constants accounting for the lateral interaction. Note that  $k_d(C)$  increases with increasing  $C$  at  $C > C_*$ . This dependence of  $k_d(C)$  on  $C$  has been introduced in order to describe our observation that after termination of adsorption weak desorption was observed only near saturation.

In order to evaluate the applicability of the proposed model, we use it to fit the kinetics of PLL adsorption on carboxyl-terminated SAM on gold (Figure 7). The fitting process, with

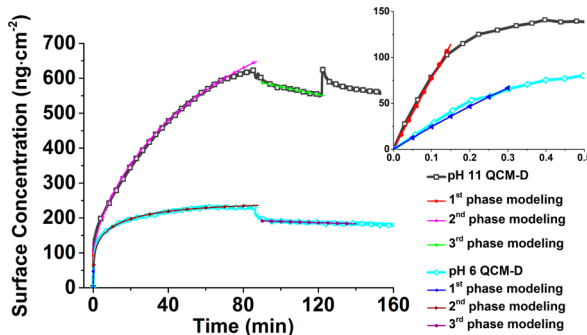


**Figure 7.** Kinetic model fitting of PLL surface concentration as a function of time during PLL adsorption on carboxyl-terminated SAM on gold. Surface concentration was calculated by using the Sauerbrey equation from the third overtone of the QCM-D signal. The kinetics exhibits three phases including the initial rapid adsorption, slow nonlinear adsorption, and desorption due to the buffer rinsing step. The flow of PLL solution into QCM-D chamber was terminated at  $t \approx 70$  min, and the substrate was left to incubate from  $t \approx 70$  to  $t \approx 85$  min. The adsorption behavior at  $t \approx 85$  min was not included in the kinetic model fitting because the corresponding flow conditions were poorly defined. The inset shows the graph of adsorption phase for the first 0.5 min of PLL adsorption at pH 11 and 6.

the aim to obtain the model parameters, started at the third phase of the kinetics, where only desorption occurred since only buffer solution was injected into the chamber to rinse the bulk solution away from the system ( $c = 0$ ). During this phase, the fitting was limited to the nearly linear region, and the values of  $k_a^o$ ,  $B$ , and  $n$  were obtained as shown in Table 1. These values were then used to fit the first two phases of the kinetics to determine the other parameters. The values of  $C_*$  and  $C_{\max}$  were retrieved from the experimental data from the transition points between the first and second phase of the kinetics and between the second and the third phase of the kinetics, respectively. The value of  $C_*$  was then used to determine the values of  $k_a^o$  from the nearly linear slope at the first phase of the kinetics. Lastly, the values of  $c$  and  $m$  were determined from the curve fitting of the second phase of the kinetics using the values of previously determined parameters. Table 1 shows that the values of  $k_a^o$  depends on the pH condition ( $k_a^o = 400$  and  $129 \text{ min}^{-1}$  at pH 11 and 6, respectively), which explains the difference in the resulting values critical concentration  $C_*$  ( $C_* = 102.8$  and  $65.9 \text{ ng cm}^{-2}$  at pH 11 and 6, respectively). Similar to  $k_a^o$ , the influence of pH on  $k_d$  is also significant ( $k_d = 0.0019$

and  $0.0009 \text{ min}^{-1}$  at pH 11 and 6, respectively). Since the values of  $k_a^o$  are about 2-fold higher compared to  $k_d$  for both pH conditions, the PLL adsorption is mainly irreversible, consistent with previous report.<sup>53</sup> The values of  $C_{\max}$  were higher at pH 11 ( $C_{\max} = 1200 \text{ ng cm}^{-2}$ ) compared to pH 6 ( $C_{\max} = 255 \text{ ng cm}^{-2}$ ), consistent with their respective  $k_a^o$  and  $C_*$  values.

In analogy with protein and vesicles, the first phase of PLL adsorption is expected to be limited by diffusion, and assuming that the channel geometry is that of a rectangular slab, the corresponding adsorption rate can be identified with the PLL diffusion flux toward the surface<sup>54</sup>

$$J = \left( \frac{3v_0 D^2}{ax} \right)^{1/3} c \quad (4)$$

where  $v_0$  is the average flow velocity,  $D$  is the diffusion coefficient,  $a$  is the cell size in the direction perpendicular to the wall adsorbing HA, and  $x$  is the coordinate along the channel ( $x = 0$  corresponds to the boundary between the areas uncovered and covered by PLL). The analysis of the corresponding diffusion length can be found in Supporting Information section S5.

In order to explore the effect of flow rate on the kinetics of PLL adsorption, we performed measurements at two carrier flow rates, 45 and  $100 \mu\text{L}/\text{min}$ , at pH 6 and pH 11 (Figure 8).

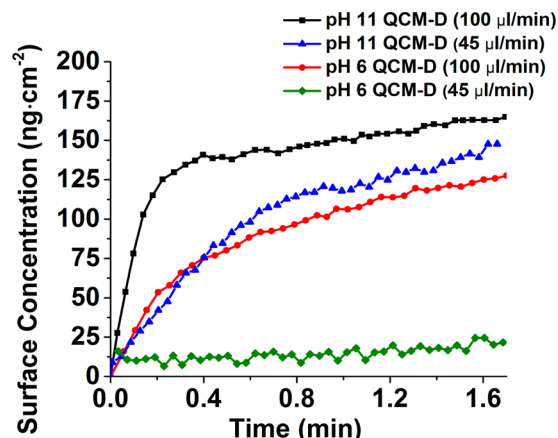


**Figure 8.** Influence of flow rate on the rate of PLL adsorption onto a carboxyl-terminated gold surface. PLL surface concentration, calculated from the third overtone of QCM-D by using the Sauerbrey equation, is shown as a function of time for PLL adsorption on carboxyl-terminated SAM on gold at two different flow rates, 45 and  $100 \mu\text{L}/\text{min}$  at pH 11 and pH 6.

The influence of flow rate is apparent at both pH conditions, with decreased adsorption rate at reduced flow rate, which in turn led to longer time duration for the concentration to reach the transition point,  $C_*$ , for adsorption process to shift from the first to the second phase. Noticeably, the PLL adsorption at pH 6 at the reduced flow rate did not manage to reach  $C_*$  within the 1.6 min time range, indicating significant influence of flow

**Table 1.** Model Parameters Obtained from Fitting the Experimentally Measured Kinetics of PLL Adsorption on Carboxyl-Terminated SAM on Gold (Figure 7)

pH	$k_a^o (\text{min}^{-1})$	$A (\text{cm}^2 \text{ ng}^{-1})$	$m$	$k_d (\text{min}^{-1})$	$B (\text{cm}^2 \text{ ng}^{-1})$	$n$	$C_{\max} (\text{ng cm}^{-2})$	$C_* (\text{ng cm}^{-2})$	$c (\text{ng cm}^{-2})$
11	400	2.37	0.10	0.0019	0.00008	1	1200	102.80	2.0
6	129	0.30	0.50	0.0009	0.00008	1	255	65.86	2.0

rate on the PLL adsorption rate. However, the change in the initial adsorption rate did not exactly commensurate with eq 4, which assumes that the channel geometry is that of a rectangular slab while this is in fact an approximation of the specific geometry of the measurement chamber used in the QCM-D experiments. The significant influence of flow rate on the PLL adsorption on a surface provides another avenue to control the rate of PLL adsorption on a surface for coating applications and supports the importance of kinetics in the adsorption and reconfiguration processes.

## ■ DISCUSSION

In this study, the pH of PLL solution was varied from pH 2 to 12 in order to analyze the effect of the corresponding variation in the electrostatic charges on both the PLL and the substrates on the adsorption rate and degree of adsorption. It is generally accepted that intermolecular electrostatic attraction between PLL molecules and the surface and repulsion among adjacent PLL molecules determine the specifics of polyelectrolyte adsorption onto surfaces.<sup>18,20,26,27</sup> According to this hypothesis, significant PLL adsorption is expected to occur only within the pH range between the IEP of the substrate and the  $pK_a$  of PLL, provided that the net electrostatic charges of PLL and the substrate share opposite polarity and therefore experience electrostatic attraction.<sup>20</sup> With increasing charge density of the surface in response to pH change, the amount of oppositely charged PLL required to neutralize the surface charge, in order to maintain electroneutrality, increases accordingly resulting in increasing PLL uptake on the surface. By varying solution pH, the amount of PLL or other type of polyelectrolytes uptake on the surface can be controlled.<sup>55</sup> PLL has  $pK_a$  values ranging between 9 and 11,<sup>4,20,27,40,41</sup> while the IEP of silica, carboxyl-, and amine-functionalized gold surfaces are about 4, 6, and 7.5, respectively.<sup>39,42–45</sup> Hence, from the perspective of electrostatic interaction, significant PLL adsorption on silica, carboxyl-, and amine-functionalized surface is expected to occur at moderate pH conditions from about pH 4 to pH 11 for silica, pH 6 to pH 11 for a carboxyl-functionalized surface, and pH 7.5 to pH 11 for a amine-terminated surface, i.e., corresponding to the ranges where electrostatic attraction between PLL molecules and silica surface provides significant driving force for adsorption.

Interestingly, the final  $\Delta f$  values at the end of the adsorption phase on all three surfaces at different pH condition do not neatly correspond to the prediction based only on electrostatic interaction. Significant PLL adsorption was observed at pH condition in which electrostatic repulsion is expected to occur between PLL and the silica or AUT-functionalized surfaces. These results support that PLL adsorption onto all three surfaces is controlled by the balance between electrostatic and nonelectrostatic interaction.<sup>34</sup> A molecular modeling study has previously attributed PLL adsorption onto silica glass to hydrogen bonding,<sup>22</sup> while hydrophobic interaction has been reported to contribute to PLL adsorption onto hydrophobic PDMS<sup>21</sup> and hydrophilic silica<sup>28</sup> surfaces. Hence, these nonelectrostatic interactions might influence PLL adsorption onto the three substrates in cooperation or competition with electrostatic interaction depending on the environmental parameters. The second explanation for the recorded PLL adsorption at unfavorable pH condition is that interfacial electrostatic charges are heterogeneously distributed on the surface of the substrates and PLL molecules, and therefore the polarities of net charges of each discrete functional groups on PLL and substrates are distinctive. Since adsorption is a short-

range process, it is determined by the charge density and polarity of the local adsorption sites.<sup>28,31</sup> At interfacial scale, interactions between the charged functional groups occur between amine groups in every PLL molecules with corresponding functional groups on the surfaces (e.g., hydroxyl in silica). Hence, nonuniform charge distribution in PLL and polar surfaces permits PLL to adsorb on favorable local adsorption sites on the surface, although the net charge of the whole substrate may be unfavorable toward PLL adsorption. Moreover, the heterogeneity of adsorption sites may explain the inhomogeneous PLL adlayer formed at pH unfavorable to adsorption (Figure 5). The trend in the QCM-D  $\Delta f$  and  $\Delta D$  shifts in response to PLL adsorption could therefore be explained methodically in reference to the influence of environmental pH on the net electrostatic charges on both PLL and the surfaces, which in turn affect the cooperation or competition between electrostatic and nonelectrostatic interaction in driving PLL adsorption.

The increase in solution pH causes the cationic charge density of PLL to decrease gradually until PLL turns neutral above its  $pK_a$ .<sup>1,3,6–8</sup> This decline in charge density results in gradual decline of the strength of electrostatic interaction between PLL and hydrophilic surfaces. For silica surface, from pH 2 to pH 4, the hydroxyl groups change from slightly cationic to neutral condition, and therefore PLL adsorption is expected to be absent *sans* any nonelectrostatic and localized electrostatic attraction competing against electrostatic repulsion. As pH increased from 2 to 4, the cationic charge density on both PLL and silica surfaces decreases, and hence electrostatic repulsion is expected to gradually decrease which permits nonelectrostatic attraction to promote higher PLL adsorption on the surface. Interestingly, the  $\Delta f$  shift decreased from pH 2 to 3 and then increased at pH 4, in contrast to the predicted electrostatic interaction trend. These results can be rationalized by taking into account that the change in  $\Delta f$  shift also depends on the amount of associated solvent within the assembled PLL adlayer. In response to decreasing charge density with increasing pH, a lesser amount of counterions from the solvent need to be assimilated into the PLL adlayer to maintain electroneutrality, resulting in the expulsion of associated solvent and therefore lower water content with increasing pH. The decrease in the amount of associated solvent compensates the increase in amount of PLL adsorbed as solution pH rises.<sup>27,40</sup> This explanation is supported by previous findings<sup>26,56</sup> that the contribution of associated solvent to the total mass decreases with increasing pH. The contrasting effect of increasing PLL adsorption and decreasing solvent uptake is further supported by the decline in  $\Delta D$  shift, which is strongly correlated with the solvent content on the adsorbed biomolecule,<sup>57,58</sup> from pH 3 to 4 as both PLL and the silica surface decline in charge density.

From pH 4 to 10, the anionic charge density on the silica surface increases while the cationic charge density of PLL decreases gradually. Hence, within this pH range, the electrostatic attraction cooperates with nonelectrostatic attraction to enhance PLL adsorption as observed with the sudden decrease in  $\Delta f$  shift from pH 4 to 5, indicating higher PLL adsorption. Subsequently, the value of  $\Delta f$  shifts remained approximately constant from pH 5 to pH 10, with the exception of notable decrease at pH 8. These results are in agreement with a previous report in which the wet mass of a PLL adlayer (i.e., the combined mass of the assembled PLL adlayer and associated solvent) was observed to be independent

of solution pH.<sup>26</sup> The relatively constant value of  $\Delta f$  shifts or wet mass in this pH range is not surprising considering that the balance between increasing anionic charge density of silica and decreasing cationic charge density of PLL should produce relatively uniform electrostatic attraction and hence PLL adsorption. In addition, the uniform trend in total charge density may explain relatively uniform hydration of PLL adlayer observed from pH 5 to 10. The sudden increase in PLL adsorption at pH 8 possibly arises from the optimal balance between the charge density of both positive and negative charges. From electrostatic interaction perspective, maximal PLL adsorption should occur at intermediate pH in which optimal charge distribution on PLL and surfaces induce strongest electrostatic attraction. The  $\Delta f$  shift values increases again at pH 9 and 10 back to the value observed at pH 5–7, indicating the reduction in electrostatic attraction and decrease in the hydration mass of the PLL adlayer.

At pH 11, the PLL uptake experienced an unanticipated upsurge considering that the cationic charge density of PLL should have reached its minimum. Maximal PLL adsorption at pH 11 was also observed on the carboxyl-functionalized surface. These results are consistent with previous studies which report abrupt increase of PLL adsorption at pH condition near its IEP.<sup>27,56</sup> One explanation is that at its IEP<sup>4,20,27,40,41</sup> the charge density of PLL molecule reached its minimum which diminished intermolecular electrostatic repulsion, inducing conformation transition from random coil to  $\alpha$ -helix. The conformation transition, in turn, results in the reduction in the hydrodynamic radius of the PLL structure.<sup>26,48,56,59</sup> The decrease in PLL size enhances the diffusion rate of PLL to the surface (see section S5 of the *Supporting Information*) and increases the packing density of PLL molecule on the surface, resulting in enhanced PLL adsorption. On the other hand, the enhanced PLL adsorption may arise from the adsorption of large PLL aggregates on the surface as PLL self-aggregation occurs in solution due to minimal intramolecular electrostatic repulsion at pH 11.<sup>48,60</sup> PLL adsorption declines again at pH 12 as the electrostatic repulsion between the anionic PLL and surfaces induces electrostatic repulsion competes with non-electrostatic attractive forces such as hydrophobic interaction and discourage the deposition of PLL molecule on the surface.

The explanation offered above to explain the trend in QCM-D  $\Delta f$  and  $\Delta D$  shifts corresponding to PLL adsorption on silica at different solution pH can also be applied to explain the  $\Delta f$  and  $\Delta D$  shifts trend observed in the PLL adsorption on carboxyl- and amine-functionalized surface. For amine-functionalized surface, the nonelectrostatic interaction competed with electrostatic repulsion between PLL and amine-functionalized surface from pH 2 to 6 and pH 12, corresponding to the pH region at which the net charges of PLL and amine-functionalized surfaces share the same polarity. This explains the relatively lower  $\Delta f$  shifts recorded at those pH regions compared to the adsorption at the region between pH 7 and 11 where both PLL and amine-functionalized surfaces are oppositely charged and therefore experience electrostatic attraction. PLL adsorptions on amine-functionalized surfaces are relatively more uniform compared to the other two surfaces. This observation can possibly be explained by admitting that the PLL adsorption on amine-functionalized surface is primarily driven by nonelectrostatic attraction such as hydrophobic interaction since the active functional groups of both PLL and the surfaces are amine groups and therefore has greater likelihood to exert electrostatic repulsion on each other. Since

nonelectrostatic interaction is less affected by the change in environmental pH, the relative uniformity in PLL adsorption on amine-functionalized surface can be explained. Interestingly, no abrupt upsurge in PLL adsorption was observed at pH 11 on amine-functionalized surface, in contrast to the other two substrates. For carboxyl-functionalized surface, the pH regions in which electrostatic repulsion reduced the PLL adsorption driven by nonelectrostatic attraction occurred from pH 2 to 6 and pH 12. The final  $\Delta f$  shifts of PLL adlayers on the carboxyl-functionalized surface exhibit an increasing trend (or decreasing magnitude of  $\Delta f$  shifts), from pH 2 to 7, indicating a gradual decrease in PLL and associated solvent uptake with increasing pH. The result is surprising considering the expected increase in PLL adsorption in line with the decreasing strength of electrostatic repulsion competing with nonelectrostatic attraction, with the decline in the net cationic charges on both PLL and the carboxyl-functionalized surface. A possible explanation is that the increase in  $\Delta f$  shift occurs due to the decline in the hydration of the PLL adlayer with decreasing charge density since less dissolved anionic ions are required to maintain electroneutrality on the PLL adlayer. The real IEP of the carboxyl-terminated SAM used in this study may have been higher than the reported value of about 6 considering that the increasing  $\Delta f$  shift trend continues until pH 7. At pH 8, the  $\Delta f$  shifts decreased and the value of the  $\Delta f$  and  $\Delta D$  shifts remained approximately uniform until pH 10. The decrease in  $\Delta f$  shifts at pH 8 to 10 relative to pH 7 truly corresponds to an increase in PLL uptake rather than increase in hydration since the value of  $\Delta D$  shifts at this pH region remained approximately similar. The increase in PLL adsorption within this pH region can be attributed to the cooperation between electrostatic and nonelectrostatic attraction from the oppositely charged PLL and carboxyl-functionalized surfaces. An abrupt upsurge in PLL adsorption was observed at pH 11 which has been explained above. Interestingly, the PLL uptake at pH 12 still remained high which is probably due to the weak electrostatic repulsion and strong nonelectrostatic attraction between the amine and carboxyl-functionalized surface.

In the majority of the assembly processes, the buffer rinsing phase of the PLL assembly resulted in an increase in  $\Delta f$  shift and decrease in  $\Delta D$  shift which describes the removal of weakly adsorbed PLL molecules and the associated solvent from the adlayer, forming a thinner and rigid PLL adlayer on the surface. At the end of the buffer rinsing phase, solution exchange from buffer at a specific pH to near-physiological pH was performed to investigate the response of PLL adlayer assembled at different pH to a change in environments to near-physiological conditions. The expected change of PLL adlayer in response to the solution exchange depends on the change in charge density of PLL adlayer and the substrate when the local pH condition is changed to near-physiological pH. For PLL adlayer adsorbed at acidic condition, the cationic charge density of PLL adlayer is expected to decrease with the increase in pH while the opposite cases occur for PLL adsorbed at basic condition. On the other hand, the cationic charge density of all three surfaces decreases gradually from pH 2 to their respective  $pK_a$ , and then the anionic charge density increases gradually from their  $pK_a$  with increasing pH.

In all three substrates, solution exchange from acidic condition to pH 7.5 generally resulted in the increase in  $\Delta f$  shifts and decrease in  $\Delta D$  shifts corresponding to the desorption of PLL adlayers and the removal of the associated solvent, in response to the reduction in the charge density of

PLL and the expulsion of the associated solvent in order to maintain electroneutrality of the layer. On the other hand, the  $\Delta f$  and  $\Delta D$  shifts in response to the solution exchange from basic condition to pH 7.5 vary depending on the type of substrates supporting the PLL layer. For PLL layer adsorbed on silica and carboxylic-functionalized gold, solution exchange resulted in initial sudden and significant decrease in  $\Delta f$  shifts and increase in  $\Delta D$  shifts, followed by the gradual recovery of the  $\Delta f$  and  $\Delta D$  shifts signals. In contrast, PLL layer on amine-functionalized surface experienced similar and sudden change in  $\Delta f$  and  $\Delta D$  shifts with no subsequent gradual recovery of the  $\Delta f$  and  $\Delta D$  shifts. The decrease in  $\Delta f$  and increase in  $\Delta D$  shifts indicate the increase in associated solvent within the adlayer during the solution exchange. While the associated solvent is gradually expelled from the PLL layer on silica and carboxylic-functionalized surface, the PLL layer on the amine-functionalized surface retained the sudden increase in the associated solvent.

Taking into consideration the extent of hydration in this system, the QCM-D experimental data show that majority of the PLL adlayers were viscoelastic with  $\Delta D$  shifts (Figures 2B, 3B, and 4B) ranging from  $\sim 1$  to  $3.6 \times 10^{-6}$ , at the end of adsorption step, which is comparable with the previous report<sup>59</sup> describing the viscoelastic properties of a PLL adlayer on gold. In order to analyze the influence of surface chemistry and pH on the viscoelastic properties of the adlayer, we calculated the ratio  $|\Delta D/\Delta f|$  of PLL adlayer after the adsorption step at different pH values and identified that there is close agreement in this ratio on different substrates, which suggests that the viscoelasticity is not significantly affected by the surface chemistry of the substrate. On the other hand, the ratio  $|\Delta D/(\Delta f/n)|$  was observed to fluctuate and exhibit a general decreasing trend with increasing pH. This result is not surprising since viscoelasticity of an adlayer is usually associated with the degree of hydration within its structure<sup>61</sup> and therefore is expected to decrease with increasing pH, in response to decreasing amount of associated solvent within its structure, as discussed above. That is the degree of adsorption varied by substrate (and indirectly by solution pH); however, the viscoelastic properties of the adsorbate were directly influenced by the solution pH and help to explain how solution pH influences the properties of PLL adlayers in general.

## CONCLUSION

Herein, we employed QCM-D to investigate the PLL assembly across a pH range of 2–12 on three different substrates, including silica, an amine-functionalized gold, and a carboxyl-functionalized gold. QCM-D responses indicate that PLL adsorption occurred in two distinct phases on all substrates and at all pH conditions. The first phase occurred rapidly with nearly linear increase in the PLL coverage up to the critical concentration where the second phase started, with gradually decelerating adsorption, until saturation was reached. Both phases were sensitive to the carrier flow rate into the assembly chamber due to the diffusion-limited nature of PLL adsorption. The PLL adsorption was mainly irreversible as indicated by the small reduction in PLL coverage during buffer rinsing step. The adsorption kinetics was observed to be dependent on pH; however, the total wet mass, represented by QCM-D frequency shifts, appeared to be unaffected by the change in pH since the increase in pH led to compensation of increase in PLL adsorption by reduction in hydration of the adlayer. Carboxyl-functionalized surface was revealed to be the most favorable for

PLL assembly, followed by amine-functionalized surface and last, silica. The PLL adsorption on the three surfaces was governed by the interplay between the Coulombic electrostatic interactions and non-Coulombic interactions involving hydrogen bonding and hydrophobic interactions. AFM imaging showed that PLL assembly at favorable pH conditions produced complete, homogeneous, and smooth PLL adlayer, while adsorption at unfavorable pH conditions produced inhomogeneous and rough adlayer. A kinetic model describing various phases of the PLL adsorption kinetics was proposed. To summarize, our results expand the physicochemical framework for PLL adsorption on different surfaces and can potentially help to improve the fabrication of supported PLL layers for surface modification applications.

## ASSOCIATED CONTENT

### Supporting Information

More detailed information about the QCM-D experimental data (Figures S1–S3), Voigt–Voinova model analysis (Figure S4), and calculations pertaining to the kinetic analysis (section S5). The Supporting Information is available free of charge on the ACS Publications website at DOI: [10.1021/acs.jpcb.5b01553](https://doi.org/10.1021/acs.jpcb.5b01553).

## AUTHOR INFORMATION

### Corresponding Author

\*E-mail [njcho@ntu.edu.sg](mailto:njcho@ntu.edu.sg) (N.-J.C.).

### Notes

The authors declare no competing financial interest.

## ACKNOWLEDGMENTS

This work was supported by the National Research Foundation (NRF-NRFF2011-01) and the National Medical Research Council (NMRC/CBRG/0005/2012). V.P.Zh. is a recipient of the Tan Chin Tuan Exchange Fellowship at Nanyang Technological University.

## REFERENCES

- (1) Shih, I. L.; Van, Y. T.; Shen, M. H. Biomedical applications of chemically and microbiologically synthesized poly(glutamic acid) and poly(lysine). *Mini-Rev. Med. Chem.* **2004**, *4* (2), 179–188.
- (2) Shukla, S. C.; Singh, A.; Pandey, A. K.; Mishra, A. Review on production and medical applications of  $\epsilon$ -polylysine. *Biochem. Eng. J.* **2012**, *65* (0), 70–81.
- (3) Mazia, D.; Schatten, G.; Sale, W. Adhesion of cells to surfaces coated with polylysine. Applications to electron microscopy. *J. Cell Biol.* **1975**, *66* (1), 198–200.
- (4) Guo, Y.; Ma, Y.; Xu, L.; Li, J.; Yang, W. Conformational change induced reversible assembly/disassembly of poly-L-lysine-functionalized gold nanoparticles. *J. Phys. Chem. C* **2007**, *111* (26), 9172–9176.
- (5) Zhu, S.-G.; Xiang, J.-J.; Li, X.-L.; Shen, S.-R.; Lu, H.-B.; Zhou, J.; Xiong, W.; Zhang, B.-C.; Nie, X.-M.; Zhou, M.; et al. Poly(L-lysine)-modified silica nanoparticles for the delivery of antisense oligonucleotides. *Biotechnol. Appl. Biochem.* **2004**, *39* (2), 179–187.
- (6) Quirk, R. A.; Chan, W. C.; Davies, M. C.; Tendler, S. J. B.; Shakesheff, K. M. Poly(L-lysine)-GRGDS as a biomimetic surface modifier for poly(lactic acid). *Biomaterials* **2001**, *22* (8), 865–872.
- (7) Williams, R. C. Use of polylysine for adsorption of nucleic acids and enzymes to electron microscope specimen films. *Proc. Natl. Acad. Sci. U. S. A.* **1977**, *74* (6), 2311–2315.
- (8) Schuler, M.; Owen, G. R.; Hamilton, D. W.; de Wild, M.; Textor, M.; Brunette, D. M.; Tosatti, S. G. P. Biomimetic modification of titanium dental implant model surfaces using the RGDSP-peptide

- sequence: A cell morphology study. *Biomaterials* **2006**, *27* (21), 4003–4015.
- (9) Suye, S. i.; Kumon, Y.; Ishigaki, A. Immobilization of glucose oxidase on poly-(L-lysine)-modified polycarbonate membrane. *Biootechnol. Appl. Biochem.* **1998**, *27* (3), 245–248.
- (10) Ryser, H. J.-P.; Shen, W.-C. Conjugation of methotrexate to poly(L-lysine) increases drug transport and overcomes drug resistance in cultured cells. *Proc. Natl. Acad. Sci. U. S. A.* **1978**, *75* (8), 3867–3870.
- (11) Di Stefano, G.; Colonna, F. P.; Bongini, A.; Busi, C.; Mattioli, A.; Fiume, L. Ribavirin conjugated with lactosaminated poly-L-lysine: selective delivery to the liver and increased antiviral activity in mice with viral hepatitis. *Biochem. Pharmacol.* **1997**, *54* (3), 357–363.
- (12) Gac-Breton, S.; Coudane, J.; Bousta, M.; Vert, M. Norfloxacin-poly(L-lysine citramide imide) conjugates and structure-dependence of the drug release. *J. Drug Targeting* **2004**, *12* (5), 297–307.
- (13) Choi, Y. H.; Liu, F.; Kim, J.-S.; Choi, Y. K.; Jong Sang, P.; Kim, S. W. Polyethylene glycol-grafted poly-L-lysine as polymeric gene carrier. *J. Controlled Release* **1998**, *54* (1), 39–48.
- (14) Toncheva, V.; Wolfert, M. A.; Dash, P. R.; Oupicky, D.; Ulbrich, K.; Seymour, L. W.; Schacht, E. H. Novel vectors for gene delivery formed by self-assembly of DNA with poly(L-lysine) grafted with hydrophilic polymers. *Biochim. Biophys. Acta, Gen. Subj.* **1998**, *1380* (3), 354–368.
- (15) Sun, H. K.; Ji, H. J.; Cheol, O. J.; Tae, G. P. Folate receptor mediated intracellular protein delivery using PLL-PEG-FOL conjugate. *J. Controlled Release* **2005**, *103* (3), 625–634.
- (16) Hynes, S. R.; Rauch, M. F.; Bertram, J. P.; Lavik, E. B. A library of tunable poly(ethylene glycol)/poly(L-lysine) hydrogels to investigate the material cues that influence neural stem cell differentiation. *J. Biomed. Mater. Res., Part A* **2009**, *89A* (2), 499–509.
- (17) Elbert, D. L.; Herbert, C. B.; Hubbell, J. A. Thin polymer layers formed by polyelectrolyte multilayer techniques on biological surfaces. *Langmuir* **1999**, *15* (16), 5355–5362.
- (18) Picart, C.; Lavalle, P.; Hubert, P.; Cuisinier, F.; Decher, G.; Schaaf, P.; Voegel, J.-C. Buildup mechanism for poly(L-lysine)/hyaluronic acid films onto a solid surface. *Langmuir* **2001**, *17* (23), 7414–7424.
- (19) Crouzier, T.; Boudou, T.; Picart, C. Polysaccharide-based polyelectrolyte multilayers. *Curr. Opin. Colloid Interface Sci.* **2010**, *15* (6), 417–426.
- (20) Kenausis, G. L.; Vörös, J.; Elbert, D. L.; Huang, N.; Hofer, R.; Ruiz-Taylor, L.; Textor, M.; Hubbell, J. A.; Spencer, N. D. Poly(L-lysine)-g-poly(ethylene glycol) layers on metal oxide surfaces: Attachment mechanism and effects of polymer architecture on resistance to protein adsorption. *J. Phys. Chem. B* **2000**, *104* (14), 3298–3309.
- (21) Lee, S.; Spencer, N. D. Adsorption properties of poly(L-lysine)-graft-poly(ethylene glycol) (PLL-g-PEG) at a hydrophobic interface: Influence of tribological stress, pH, salt concentration, and polymer molecular weight. *Langmuir* **2008**, *24* (17), 9479–9488.
- (22) West, J. K.; Latour, R.; Hench, L. L. Molecular modeling study of adsorption of poly-L-lysine onto silica glass. *J. Biomed. Mater. Res.* **1997**, *37* (4), 585–591.
- (23) Huang, N.-P.; Michel, R.; Voros, J.; Textor, M.; Hofer, R.; Rossi, A.; Elbert, D. L.; Hubbell, J. A.; Spencer, N. D. Poly(L-lysine)-g-poly(ethylene glycol) layers on metal oxide surfaces: Surface-analytical characterization and resistance to serum and fibrinogen adsorption. *Langmuir* **2000**, *17* (2), 489–498.
- (24) Babič, M.; Horák, D.; Trchová, M.; Jendelová, P.; Glogarová, K.; Lesný, P.; Herynek, V.; Hájek, M.; Syková, E. Poly(L-lysine)-modified iron oxide nanoparticles for stem cell labeling. *Bioconjugate Chem.* **2008**, *19* (3), 740–750.
- (25) Perrino, C.; Lee, S.; Choi, S. W.; Maruyama, A.; Spencer, N. D. A biomimetic alternative to poly(ethylene glycol) as an antifouling coating: Resistance to nonspecific protein adsorption of poly(L-lysine)-graft-dextran. *Langmuir* **2008**, *24* (16), 8850–8856.
- (26) Porus, M.; Maroni, P.; Borkovec, M. Response of adsorbed polyelectrolyte monolayers to changes in solution composition. *Langmuir* **2012**, *28* (50), 17506–17516.
- (27) Jiang, M.; Popa, I.; Maroni, P.; Borkovec, M. Adsorption of poly(L-lysine) on silica probed by optical reflectometry. *Colloids Surf., A* **2010**, *360* (1), 20–25.
- (28) Hoogeveen, N. G.; Stuart, M. A. C.; Fleer, G. J. Polyelectrolyte adsorption on oxides: I. Kinetics and adsorbed amounts. *J. Colloid Interface Sci.* **1996**, *182* (1), 133–145.
- (29) Szilagyi, I.; Trefalt, G.; Tiraferri, A.; Maroni, P.; Borkovec, M. Polyelectrolyte adsorption, interparticle forces, and colloidal aggregation. *Soft Matter* **2014**, *10* (15), 2479–2502.
- (30) Hartwig, R. A.; van de Weert, M.; Østergaard, J.; Jorgensen, L.; Jensen, H. Protein adsorption at charged surfaces: The role of electrostatic interactions and interfacial charge regulation. *Langmuir* **2011**, *27* (6), 2634–2643.
- (31) Hashimoto, T.; Gamo, K.; Fukuta, M.; Zheng, B.; Zettsu, N.; Yamashita, I.; Uraoka, Y.; Watanabe, H. Control of selective adsorption behavior of Ti-binding ferritin on a SiO<sub>2</sub> substrate by atomic-scale modulation of local surface charges. *Appl. Phys. Lett.* **2011**, *99* (26), 263701.
- (32) Satriano, C.; Svedhem, S.; Kasemo, B. Well-defined lipid interfaces for protein adsorption studies. *Phys. Chem. Chem. Phys.* **2012**, *14* (48), 16695–16698.
- (33) Elter, P.; Lange, R.; Beck, U. Electrostatic and dispersion interactions during protein adsorption on topographic nanostructures. *Langmuir* **2011**, *27* (14), 8767–8775.
- (34) Borges, J.; Campiña, J. M.; Silva, A. F. Probing the contribution of different intermolecular forces to the adsorption of spheroproteins onto hydrophilic surfaces. *J. Phys. Chem. B* **2013**, *117* (51), 16565–16576.
- (35) Rabe, M.; Verdes, D.; Seeger, S. Understanding protein adsorption phenomena at solid surfaces. *Adv. Colloid Interface Sci.* **2011**, *162* (1–2), 87–106.
- (36) Tsapikouni, T. S.; Missirlis, Y. F. Protein–material interactions: From micro-to-nano scale. *Mater. Sci. Eng., B* **2008**, *152* (1–3), 2–7.
- (37) Gray, J. J. The interaction of proteins with solid surfaces. *Curr. Opin. Struct. Biol.* **2004**, *14* (1), 110–115.
- (38) Zhdanov, V.; Kasemo, B. Monte Carlo simulations of the kinetics of protein adsorption. *Surf. Rev. Lett.* **1998**, *5* (02), 615–634.
- (39) Cuddy, M. F.; Poda, A. R.; Brantley, L. N. Determination of isoelectric points and the role of pH for common quartz crystal microbalance sensors. *ACS Appl. Mater. Interfaces* **2013**, *5* (9), 3514–3518.
- (40) Burke, S. E.; Barrett, C. J. pH-responsive properties of multilayered poly(L-lysine)/hyaluronic acid surfaces. *Biomacromolecules* **2003**, *4* (6), 1773–1783.
- (41) Wang, Y.; Chang, Y. C. Synthesis and conformational transition of surface-tethered polypeptide: Poly(L-lysine). *Macromolecules* **2003**, *36* (17), 6511–6518.
- (42) Shimazu, K.; Teranishi, T.; Sugihara, K.; Uosaki, K. Surface mass titrations of self-assembled monolayers of omega-mercaptoalkanoic acids on gold. *Chem. Lett.* **1998**, *7*, 669–670.
- (43) Campiña, J. M.; Martins, A.; Silva, F. Selective permeation of a liquidlike self-assembled monolayer of 11-amino-1-undecanethiol on polycrystalline gold by highly charged electroactive probes. *J. Phys. Chem. C* **2007**, *111* (14), 5351–5362.
- (44) Smalley, J. F.; Chalfant, K.; Feldberg, S. W.; Nahir, T. M.; Bowden, E. F. An indirect laser-induced temperature jump determination of the surface pKa of 11-mercaptopoundecanoic acid monolayers self-assembled on gold. *J. Phys. Chem. B* **1999**, *103* (10), 1676–1685.
- (45) Degefa, T. H.; Schön, P.; Bongard, D.; Walder, L. Elucidation of the electron transfer mechanism of marker ions at SAMs with charged head groups. *J. Electroanal. Chem.* **2004**, *574* (1), 49–62.
- (46) Jackson, M.; Haris, P. I.; Chapman, D. Conformational transitions in poly(L-lysine): Studies using Fourier transform infrared spectroscopy. *Biochim. Biophys. Acta, Protein Struct. Mol. Enzymol.* **1989**, *998* (1), 75–79.

- (47) Mirtič, A.; Grdadolnik, J. The structure of poly-L-lysine in different solvents. *Biophys. Chem.* **2013**, *175*, 47–53.
- (48) Rodriguez-Maldonado, L.; Fernandez-Nieves, A.; Fernandez-Barbero, A. Dynamic light scattering from high molecular weight poly-L-lysine molecules. *Colloids Surf., A* **2005**, *270*, 335–339.
- (49) Guo, Y.; Xia, F.; Xu, L.; Li, J.; Yang, W.; Jiang, L. Switchable wettability on cooperative dual-responsive poly-L-lysine surface. *Langmuir* **2009**, *26* (2), 1024–1028.
- (50) Zhao, C.; Zhuang, X.; He, C.; Chen, X.; Jing, X. Synthesis of novel thermo- and pH-responsive poly(L-lysine)-based copolymer and its micellization in water. *Macromol. Rapid Commun.* **2008**, *29* (22), 1810–1816.
- (51) Voinova, M. V.; Rodahl, M.; Jonson, M.; Kasemo, B. Viscoelastic acoustic response of layered polymer films at fluid-solid interfaces: continuum mechanics approach. *Phys. Scr.* **1999**, *59* (5), 391.
- (52) Choi, J.-H.; Kim, S.-O.; Linardy, E.; Dreaden, E. C.; Zhdanov, V. P.; Hammond, P. T.; Cho, N.-J. Adsorption of hyaluronic acid on solid supports: Role of pH and surface chemistry in thin film self-assembly. *J. Colloid Interface Sci.* **2015**, *448* (0), 197–207.
- (53) Furst, E. M.; Pagac, E. S.; Tilton, R. D. Coadsorption of polylysine and the cationic surfactant cetyltrimethylammonium bromide on silica. *Ind. Eng. Chem. Res.* **1996**, *35* (5), 1566–1574.
- (54) Zhdanov, V.; Keller, C.; Glasmästar, K.; Kasemo, B. Simulation of adsorption kinetics of lipid vesicles. *J. Chem. Phys.* **2000**, *112* (2), 900–909.
- (55) Shiratori, S. S.; Rubner, M. F. pH-dependent thickness behavior of sequentially adsorbed layers of weak polyelectrolytes. *Macromolecules* **2000**, *33* (11), 4213–4219.
- (56) Porus, M.; Maroni, P.; Borkovec, M. Structure of adsorbed polyelectrolyte monolayers investigated by combining optical reflectometry and piezoelectric techniques. *Langmuir* **2012**, *28* (13), 5642–5651.
- (57) Vörös, J. The density and refractive index of adsorbing protein layers. *Biophys. J.* **2004**, *87* (1), 553–561.
- (58) Rodahl, M.; Hook, F.; Fredriksson, C.; Keller, C. A.; Krozer, A.; Brzezinski, P.; Voinova, M.; Kasemo, B. Simultaneous frequency and dissipation factor QCM measurements of biomolecular adsorption and cell adhesion. *Faraday Discuss.* **1997**, *107* (0), 229–246.
- (59) Dutta, A. K.; Nayak, A.; Belfort, G. Viscoelastic properties of adsorbed and cross-linked polypeptide and protein layers at a solid–liquid interface. *J. Colloid Interface Sci.* **2008**, *324* (1–2), 55–60.
- (60) Lee, W. I.; Schurr, J. M. Laser light scattering studies of poly(L-lysine HBr) in aqueous solutions. *J. Polym. Sci., Polym. Phys. Ed.* **1975**, *13* (5), 873–888.
- (61) Höök, F.; Kasemo, B.; Nylander, T.; Fant, C.; Sott, K.; Elwing, H. Variations in coupled water, viscoelastic properties, and film thickness of a mefp-1 protein film during adsorption and cross-linking: A quartz crystal microbalance with dissipation monitoring, ellipsometry, and surface plasmon resonance study. *Anal. Chem.* **2001**, *73* (24), 5796–5804.